Nuclear Inst. and Methods in Physics Research B xxx (xxxx) xxx–xxx

Contents lists available at ScienceDirect

Nuclear Inst. and Methods in Physics Research B

journal homepage: www.elsevier.com/locate/nimb

Relativistic atomic structure calculations of heavy targets for inelastic collisions

A.M.P. Mendez*, C.C. Montanari, D.M. Mitnik

Instituto de Astronomía y Física del Espacio, CONICET – Universidad de Buenos Aires, Buenos Aires, Argentina

ARTICLE INFO

Keywords:
Relativistic atomic structure
Dirac equation
Fermi Energies
Inelastic collisions

ABSTRACT

Fully relativistic atomic structure calculations for Zr, Nb, Pd, Gd, Er, Hf, Ta, Os, and Pt are presented here. The description of these atoms requires the solution of the Dirac equation. The electron binding energies attained are compared with experimental values, achieving excellent overall agreement for the inner shells. Discrepancies in the outer shell binding energies between the isolated atom and the solid are discussed, giving special attention to the open $4f$–subshell. Based on the present calculations, we analyzed the valence shell of the nine elements studied here and propose theoretical values for the Wigner-Seitz radio.

1. Introduction

The study of energy loss processes by ions in solids is a powerful tool in many areas of basic science and material technology. Tables and codes resulting from semiempirical calculations are available for a large combination of ions and targets [1,2]. However, inelastic scattering calculations of heavy targets remains a difficult task since it becomes necessary to account for the relativistic effects, which are important not only for the inner electrons but also to define the outer–shell binding energies.

In the present work, efforts are made to accurately describe the atomic structure of heavy atoms using a fully relativistic method. The goal of this contribution is to provide a set of reliable wave functions and binding energies to be used in atomic collision calculations. There are various methods that consider such quantities as input data for computing inelastic processes. For example, the shellwise local plasma approximation (SLPA) allows one to compute the different moments of energy loss [3–6] knowing only the orbital densities and binding energies of the target electrons in the ground state.

The description of targets that involve the $4f$–electrons is particularly interesting. This group of electrons plays an important role in the energy loss, as valence or subvalence electrons, or even as a quasi-free electron gas, enhancing the energy loss at very low energies (see, for example, [7]). In this contribution, three different groups of atoms of the periodic table are considered: transition metals with $4d$-electrons in the valence shell (Zr, Nb, and Pd), lanthanides with open $4f$-subshell (Gd and Er), and heavy transition metals with fourteen $4f$-electrons in the subvalence shell (Hf, Ta, Os, and Pt). The present theoretical results and the different characteristics of these groups of elements are analyzed in the following sections. Atomic units are used throughout this work.

2. Theory

The description of the atomic relativistic states of heavy atoms is obtained by solving the many–electron Dirac Hamiltonian,

$$H = H' + H_{\text{Breit}}(i, j) + H_{\text{QED}}, \tag{1}$$

where $H_{\text{Breit}}(i, j)$ is the Breit term and H_{QED} accounts for quantum electrodynamic effects.

$$H' = \sum_i \left[h_i^{\text{D}} - \frac{Z}{r_i} \right] + \sum_{i<j} \frac{1}{r_{ij}}, \tag{2}$$

where h_i^{D} is the single-particle kinetic Dirac Hamiltonian. The other terms in (2) correspond to the nuclei-electron and electron–electron interaction. The HULLAC code package (see Ref. [8] and references therein for more details) was used to solve numerically the Dirac equation. In this suite, the RELAC code is used to calculate first order energies and wave functions by implementing the relativistic parametric potential method. This method employs the first order relativistic perturbation theory along with the central field approximation, allowing the Hamiltonian H' to be written as an unperturbed term

$$H_0 = \sum_i h_i^{\text{D}} + U(r_i), \tag{3}$$

plus a first orden perturbation

* Corresponding author.
E-mail address: alemendez@iafe.uba.ar (A.M.P. Mendez).

https://doi.org/10.1016/j.nimb.2019.02.002
Received 27 August 2018; Received in revised form 12 November 2018; Accepted 1 February 2019

Table 1
Present theoretical and experimental [9] electron binding energies and $\langle r \rangle$ values in a.u. of Zr, Nb, Pd, Gd, Er, Hf, Ta, Os and Pt.

nljm	E^{expt}	E^{th}	$\langle r \rangle^{th}$	E^{expt}	E^{th}	$\langle r \rangle^{th}$	E^{expt}	E^{th}	$\langle r \rangle^{th}$
		Zr			Nb			Pd	
1*s*	661.40	651.34	0.0372	697.71	685.57	0.0362	894.83	880.77	0.032
2*s*	93.05	90.40	0.163	99.15	95.94	0.159	132.4	128.7	0.138
$2p_-$	84.78	82.78	0.139	90.59	87.85	0.136	122.4	119.7	0.117
$2p_+$	81.69	79.66	0.144	87.13	84.40	0.140	116.6	113.9	0.122
3*s*	15.81	14.76	0.460	17.15	16.08	0.445	24.68	23.16	0.382
$3p_-$	12.62	11.95	0.456	13.82	13.12	0.441	20.58	19.52	0.374
$3p_+$	12.12	11.45	0.467	13.25	12.55	0.452	19.56	18.53	0.385
$3d_-$	6.656	6.505	0.450	7.53	7.41	0.431	12.51	11.98	0.359
$3d_+$	6.571	6.413	0.454	7.434	7.300	0.435	12.32	11.78	0.363
4*s*	1.86	1.99	1.20	2.07	2.19	1.14	3.20	3.23	0.937
$4p_-$	1.05	1.21	1.32	1.20	1.35	1.26	2.05	2.09	1.01
$4p_+$	0.996	1.14	1.36	1.13	1.26	1.29	1.87	1.91	1.04
$4d_-$		0.103	3.15		0.121	2.62		0.216	1.61
$4d_+$		0.100	3.29		0.116	2.73		0.198	1.67
5*s*		0.182	4.34		0.189	4.20			
		Gd			Er			Hf	
1*s*	1846.2	1834.6	0.0220	2112.5	2114.2	0.0203	2401.6	2400.4	0.0190
2*s*	307.8	303.1	0.0927	358.3	353.7	0.0859	414.19	408.98	0.0798
$2p_-$	291.4	288.9	0.0773	340.4	337.5	0.0714	394.64	390.26	0.0662
$2p_+$	266.2	263.2	0.0841	307.1	303.3	0.0788	351.4	346.4	0.0740
3*s*	69.12	67.00	0.245	81.07	79.34	0.225	95.58	93.55	0.208
$3p_-$	62.03	60.48	0.234	73.72	72.00	0.215	86.91	85.40	0.198
$3p_+$	56.74	55.29	0.247	66.59	64.92	0.229	77.43	75.97	0.213
$3d_-$	44.903	43.633	0.219	53.40	51.91	0.202	63.06	62.14	0.187
$3d_+$	43.716	42.492	0.224	51.78	50.38	0.206	61.08	60.12	0.191
4*s*	13.91	13.36	0.554	16.53	15.62	0.507	19.8	18.8	0.468
$4p_-$	10.5	10.8	0.565	13.46	12.69	0.516	16.10	15.46	0.474
$4p_+$	9.96	9.65	0.596	11.77	11.06	0.549	13.99	13.28	0.508
$4d_-$	–	5.405	0.635	6.159	6.186	0.580	8.08	7.81	0.530
$4d_+$	5.240	5.193	0.646	6.159	5.892	0.592	7.772	7.418	0.542
5*s*	1.3	2.0	1.37	1.86	1.95	1.26	2.36	2.55	1.12
$5p_-$	0.74	1.3	1.54	1.13	1.16	1.41	1.4	1.6	1.24
$5p_+$	0.74	1.1	1.65	0.908	0.954	1.51	1.10	1.28	1.35
$4f_-$	0.32	0.32	1.01	–	0.18	0.851	0.584	0.725	0.666
$4f_+$	0.32	0.30	1.05	0.17	0.14	0.876	0.522	0.660	0.679
6*s*		0.40	3.79		0.19	3.43		0.214	3.83
$5d_-$		0.35	2.77					0.125	2.27
$5d_+$		0.34	2.84					0.109	3.13
		Ta			Os			Pt	
1*s*	2477.4	2479.9	0.0186	2714.6	2718.1	0.0177	2880.9	2881.6	0.0171
2*s*	429.30	423.71	0.0784	476.55	471.11	0.0743	510.07	504.78	0.0718
$2p_-$	409.23	404.55	0.0649	455.13	450.34	0.0614	487.76	483.25	0.0591
$2p_+$	363.1	357.6	0.0728	399.49	393.93	0.0696	424.96	419.70	0.0676
3*s*	99.51	97.33	0.205	112.0	109.9	0.193	121.1	118.8	0.187
$3p_-$	90.73	88.97	0.194	102.6	100.9	0.183	111.2	109.4	0.177
$3p_+$	80.63	78.86	0.209	90.29	88.54	0.199	97.20	95.37	0.192
$3d_-$	65.89	64.63	0.184	74.64	73.56	0.174	80.92	79.83	0.168
$3d_+$	63.76	62.47	0.188	72.03	70.92	0.178	77.98	76.83	0.172
4*s*	20.70	19.78	0.459	24.19	23.12	0.432	26.66	25.53	0.416
$4p_-$	17.03	16.35	0.465	20.18	19.36	0.436	22.38	21.55	0.419
$4p_+$	14.73	14.01	0.499	17.30	16.46	0.471	19.09	18.22	0.453
$4d_-$	8.742	8.353	0.519	10.77	10.29	0.484	12.19	11.70	0.463
$4d_+$	8.320	7.931	0.530	10.23	9.763	0.496	11.56	11.09	0.474
5*s*	2.56	2.72	1.09	3.1	3.4	0.995	3.737	3.829	0.942
$5p_-$	1.55	1.71	1.20	2.1	2.2	1.09	2.40	2.53	1.02
$5p_+$	1.20	1.37	1.31	1.64	1.70	1.19	1.90	1.94	1.12
$4f_-$	0.864	0.990	0.631	1.96	1.99	0.551	2.74	2.75	0.513
$4f_+$	0.794	0.916	0.642	1.86	1.89	0.560	2.62	2.62	0.520
6*s*		0.218	3.75		0.237	1.96		0.250	3.30
$5d_-$		0.130	2.61		0.194	2.18		0.250	1.71
$5d_+$		0.112	2.97		0.159	3.46		0.200	1.88

$$H_1 = \sum_{i<j} \frac{1}{r_{ij}} - \sum_i \left[\frac{Z}{r_i} + U(r_i)\right], \tag{4}$$

while the Breit term and the QED effects are added to the energies as second order perturbations. The parametric potential $U(r_i)$ describes in a simple maner the screening of the charge distribution and is determined by minimizing the first order configuration average energies. The parametric potential method is implemented within the configuration interaction (CI) scheme, i.e., the potential is minimized for different groups of configurations, clustered by similar energies and the same parity. The Hamiltonian H', is then constructed on the basis of the mixed configurations included in the $U(r_i)$ calculation, allowing to take into account, in this way, correlation effects.

The expectation value of any operator $\widehat{A}$ is given by

$$\langle \widehat{A} \rangle = \int_0^\infty [P^*(r)\widehat{A}\,P(r) + Q^*(r)\widehat{A}\,Q(r)]\,dr \tag{5}$$

where $P(r)$ and $Q(r)$ are the large and small components of the Dirac spinors, respectively. For the relativistic orbitals, we use the notation $nl_\pm$, which means nl_j, where the index $j = l \pm 1/2$ is referred as $\pm$.

3. Results

3.1. Binding energies and mean radii for isolated atoms

Configuration interaction effects are very important for the atoms considered here. Therefore, details about the mixing included in our calculations deserve special consideration. The transition elements examined here are arranged into two sets according to their period; Zr (40), Nb (41), Pd (46), in one group, and Hf (72), Ta (73), Os (76), Pt (78) in the other. In both groups, the *nd* subshell of the atom is being filled, with $n = 4$ for the first group, and $n = 5$ for the second. The ground configuration of these elements are of the type $nd^a(n+1)s^b$, where for the first set of atoms $a = 2, 4, 10$ and $b = 2, 1, 0$, while for the second, $a = 2, 3, 6, 9$ and $b = 2, 2, 2, 1$. The *nd* and $(n+1)s$ electrons have similar binding energies. Therefore, the $nd^a(n+1)s^2$, $nd^{a+1}(n+1)s^1$ and nd^{a+2} configurations have comparable energies. Since these configurations have the same parity, they must be included in the mixing configuration calculations. For example, for Zr, in which the ground state is [Kr]$4d^25s^2$, we included mixing between $4d^25s^2$, $4d^35s$, and $4d^4$. Similarly, for Pt, the ground state is [Xe] $5d^96s$, and we included mixing interaction with the $5d^{10}$ configuration.

The lanthanides atoms considered for examination – Gd (64) and Er (68) –, have ground configurations [Xe] $4f^75d6s^2$ and [Xe] $4f^{12}6s^2$, respectively. In the case of Gd, we also need to include interactions between the unfilled $4f$ and the $5d$ orbitals. Then, the most important contributions to the configuration interaction are given by the mixing of the $4f^75d6s^2$ and the $4f^86s^2$ configurations. In the case of Er, the main mixing is produced by the $4f^{12}6s^2$ and the $4f^{12}5d6s$ configurations.

The relativistic binding energies obtained from the present calculations are displayed in Table 1. The mean values $\langle r \rangle$, defined by Eq. (5), are also given in the table. The binding energies for the nine atoms studied here are displayed in Figs. 1 and 2 using filled symbols. The experimental binding energies for solids, compiled by Williams [9], are included in these figures with hollowed circles, and the theoretical binding energies yielded by Desclaux [10] implementing the Dirac-Fock method are shown with × symbols.

The agreement between the present theoretical results and the experimental binding energies is very good overall. Since Figs. 1 and 2 display the binding energies in a five-order magnitude range, it is not possible to discern the discrepancies between the data listed in Table 1 and the corresponding results of Ref. [10]. In order to assess the differences, the ratios $E^{\text{expt}}/E^{\text{th}}$ and $E^{\text{expt}}/E^{[10]}$ between the experimental and both of the theoretical binding energies are presented in Fig. 3, with black solid and red dashed lines, respectively. The binding energies we obtained for Zr and Nb show an overall agreement of about

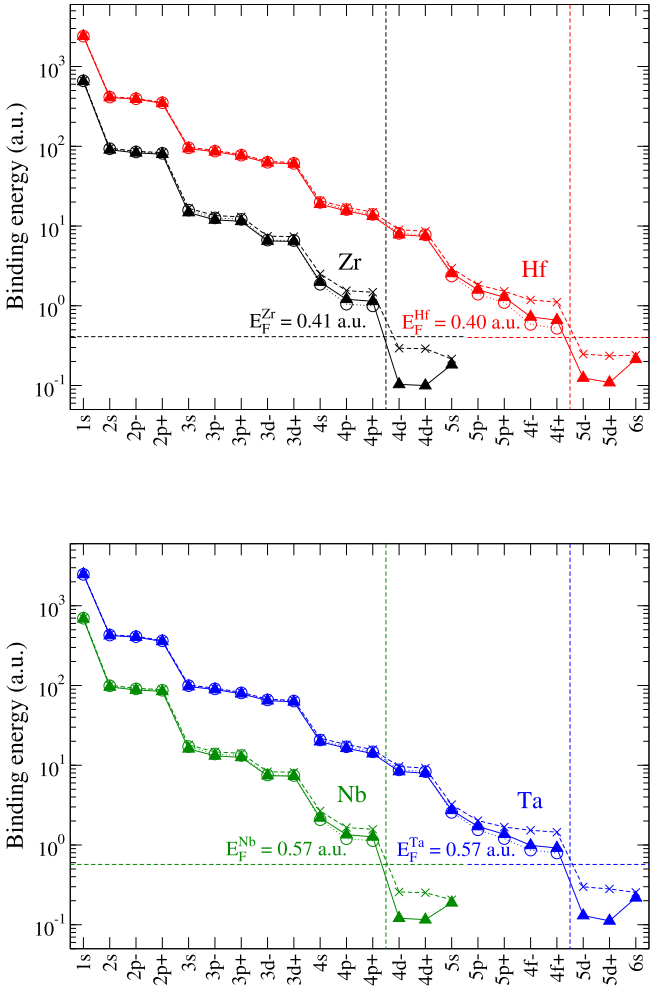

Fig. 1. Present theoretical relativistic binding energies (filled symbols), Dirac-Fock relativistic results [10] (× symbols) and experimental values [9] (hollowed circles) of Zr, Nb, Hf and Ta.

4% for all the shells, except for the subvalence $4p$. Similarly, the results obtained for Hf and Ta agree with the experimental values in ∼ 3%, except the $5p$ and $4f$ subshells. The lanthanides Gd and Er also present agreement of about 3%, with exception of the outermost subshells $5s$, $5p$ and $4f$. Surprisingly, for the transition metals Pd, Os and Pt, whose *nd* subshells are more filled, the agreement is better than 3% for all the subshells, even the subvalence $4p$ of Pd and the $5p$, $4f$ of Os and Pt. In all the cases, the present results describe the experimental data more accurately than [10].

3.2. Discussion on the values for solids

In this work, we calculated binding energies for isolated atoms (gases). However, the experimental energies considered for comparisons [9] correspond to measurements in solids (ionization of the bound electrons). As expected, the main gas-solid discrepancies are found for the outer shells. The electrons in the orbits adjacent to the conduction band in a solid are loosely bound, compared to the tightly bounding of the electrons in an isolated atom. The vertical dashed lines in Figs. 1 and 2 separate the bound and the valence electrons. The present results give a good insight about the number of electrons in the free electron gas (FEG) of solids, which are particularly relevant in stopping power calculations.

The FEG is characterized by the density of electrons, or equivalently by the Wigner-Seitz radio r_S, directly related to the Fermi energy E_F. To obtain these values, a thorough analysis of the binding energies is

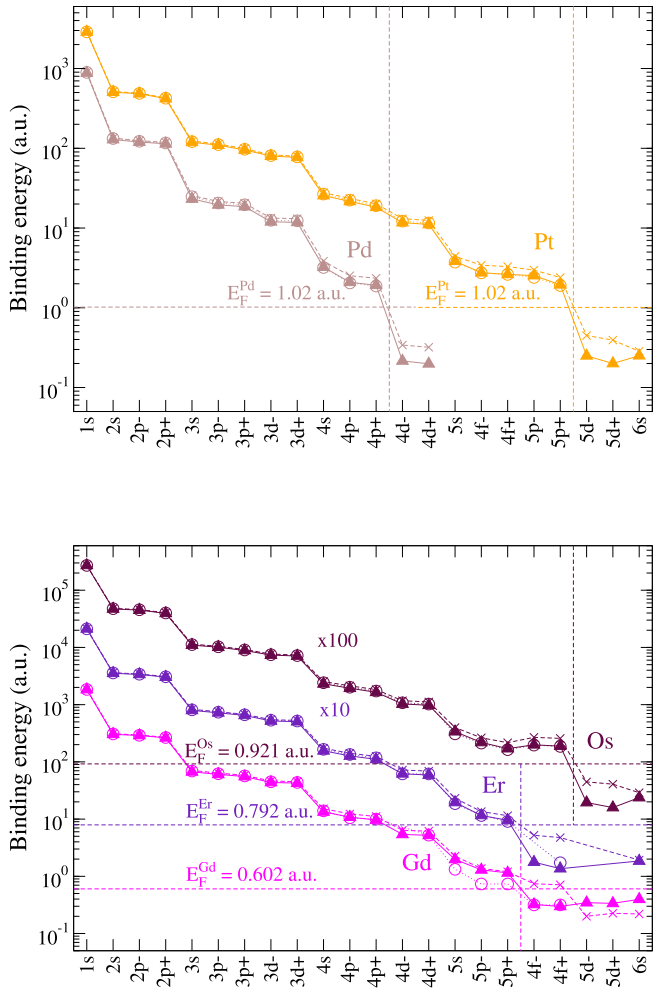

Fig. 2. Present theoretical relativistic binding energies (filled symbols), Dirac-Fock relativistic results [10] (× symbols) and experimental values [9] (hollowed circles) of Pd, Gd, Er, Os and Pt.

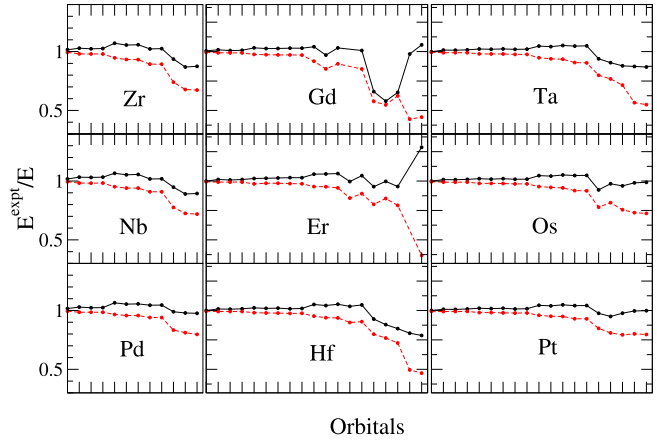

Fig. 3. Ratio between experimental and theoretical binding energies; E^{expt}/E^{th} is shown with black solid line and $E^{expt}/E^{[10]}$ with red dashed line. The orbitals correspond to the given in Figs. 1 and 2.

needed to determine the actual number of electrons belonging to the FEG. Our theoretical results for each target are displayed in Table 2. For Zr, Nb, Hf, and Ta, the experimental r_S are derived from the optical energy loss function [11–14], resulting in r_S^{exp} = 2.18, 1.72, 2.12 and 1.73, respectively. Our theoretical results agree within 4% with these values. On the other hand, no experimental data was found for Gd and Er, while for Pd, Os and Pt the number of electrons in the FEG are subject of discussion. For example, for Pd, assuming that only 6 electrons belong to the valence band (part of the 4*d* electrons), the Fermi energy is E_F = 0.74 a.u.. Otherwise, considering the whole subshell as 10 electrons in the conduction band, the corresponding value is E_F = 1.02 a.u. (displayed in Table 2). Analogously, for Pt, assuming 6 valence electrons (part of the 5*d* electrons) produces E_F = 0.72 a.u., instead of E_F = 1.02 a.u., obtained with the assumption of 10 electrons belonging to the valence shell.

Table 2
Present theoretical FEG parameters for Zr, Nb, Pd, Gd, Er, Hf, Ta, Os, and Pt: Z, nuclear charge, N_e, the number of electrons in the FEG; r_S, the Wigner-Seitz radio; and E_F, the Fermi energy.

	Zr	Nb	Pd	Gd	Er	Hf	Ta	Os	Pt
Z	40	41	46	64	68	72	73	76	78
N_e	4	5	10	10	14	4	5	8	10
r_S	2.11	1.80	1.34	1.75	1.52	2.14	1.80	1.41	1.34
E_F	0.41	0.57	1.02	0.602	0.792	0.40	0.57	0.921	1.02

For the atoms studied here, we noted that the binding energies of the outermost electrons lay below the Fermi energies. However, the lower curves in Fig. 2 show a clear contrast between the lanthanides and the rest of the atoms. For Gd, Table 2 shows that the 4*f* electrons have very close energies to the outer 5*d* and 6*s* subshells. This feature lead us to consider them as part of the FEG. The same conclusion is attained for Er. As stated previously, the specific determination of the valence and subvalence shells are important in solid state physics. Particularly, admitting the 4*f* electrons into the FEG allows to explain [15,16] the main features of recent low-energy measurements of stopping power of protons in Gd [7].

4. Summary

Binding energies and wave functions were computed for several atoms having nuclear charges ranging between 41 and 78, by solving the fully-relativistic Dirac equation with the set of codes HULLAC, which includes the Breit term and QED corrections. The agreement between the present theoretical results and the experimental values is excellent, with the sole exception of the subvalence shells of some transition elements. The present results are found to be closer to the experimental ones than other theoretical computations. The fact that the theoretical calculations have been performed for isolated atoms, and the experimental values correspond to binding energies of solids, accounts for the differences encountered. Our results allow to propose theoretical Wigner-Seitz radii for all the targets. We found a particular feature for the lanthanides, which indicates that the 4*f* electrons belong to the free electron gas.

Acknowledgements

The authors acknowledge the financial support from the following institutions of Argentina: Consejo Nacional de Investigaciones Científicas y Técnicas (CONICET), Agencia Nacional de Promoción Científica y Tecnológica (ANPCyT), and Universidad de Buenos Aires (UBA).

References

[1] Available codes for stopping power calculations can be found in https://www-nds.iaea.org/stopping/stopping_prog.html.
[2] H. Paul, A. Schinner, At. Data Nucl. Data Tables 85 (2003) 377–452.

[3] C.C. Montanari, J.E. Miraglia, Adv. Quantum Chem. 65 (2013) 165.
[4] C.C. Montanari, C.D. Archubi, D.M. Mitnik, J.E. Miraglia, Phys. Rev. A 79 (2009) 032903.
[5] C.C. Montanari, D.M. Mitnik, J.E. Miraglia, Rad. Eff. Defects Sol. 166 (2011) 338.
[6] M. Oswal, Sunil Kumar, Udai Singh, G. Singhe, K.P. Singh, D. Mehta, D. Mitnik, C.C. Montanari, T. Nandi, Nucl. Instr. Meth. Phys. Res. B 416 (2018) 110.
[7] D. Roth, B. Bruckner, M.V. Moro, S. Gruber, D. Goebl, J.I. Juaristi, M. Alducin, R. Steinberger, J. Duchoslav, D. Primetzhofer, P. Bauer, Phys. Rev. Lett. 118 (2017) 103401.
[8] A. Bar-Shalom, M. Klapisch, J. Oreg, J. Quant. Spectrosc. Radiat. Transf. 71 (2001) 169.
[9] G. Williams in http://xdb.lbl.gov/Section1/Sec_1-1.html.
[10] J.P. Desclaux, At. Data Nucl. Data Tables 12 (1973) 311.
[11] W.S.M. Werner, K. Glantschnig, C. Ambrosch-Draxl, J. Phys. Chem. Ref. Data 38 (2009) 1013–1092.
[12] D.W. Lynch, C.G. Olson, J.H. Weaver, Phys. Rev. B 11 (1975) 3617.
[13] D. Isaacson, Compilation of RS values, New York University Rep. No. 02698 (National Auxiliary Publication Service, NY 1975).
[14] P. Romaniello, P.L. de Boeij, F. Carbone, D. van der Marel, Phys. Rev. B 73 (2006) 075115.
[15] C.C. Montanari, J.E. Miraglia, Phys. Rev. A 96 (2017) 012707.
[16] A.M.P. Mendez, C.C. Montanari, D.M. Mitnik, J.E. Miraglia, to be published.